Organic Electronics 13 (2012) 506–513

Contents lists available at SciVerse ScienceDirect

Organic Electronics

journal homepage: www.elsevier.com/locate/orgel

Direct structuring of C60 thin film transistors by photo-lithography under ambient conditions

H. Kleemann *, A.A. Zakhidov, M. Anderson, T. Menke, K. Leo, B. Lüssem

Institut für Angewandte Photophysik, Technische Universität Dresden, 01062 Dresden, Germany

ARTICLE INFO

Article history:
Received 3 November 2011
Received in revised form 29 November 2011
Accepted 5 December 2011
Available online 2 January 2012

Keywords:
Organic thin film transistors
Photo-lithography on organic semiconductors
Contact resistances
Scaling laws of OTFTs

ABSTRACT

Direct structuring techniques are an indispensable need for future low-cost applications of organic semiconductor materials in e.g. active matrix displays or integrated circuits. We demonstrate direct structuring of a small molecule organic semiconductor by a photo-lithography lift off process under ambient conditions. To show compatibility of this process, we fabricate organic thin film transistors (OTFT) containing the benchmark electron transporting semiconductor C60 as active material in a top-contact geometry. C60 as electron transporting semiconductor serves as good indicator for contamination and degradation caused by the structuring procedure. To disclose influences of structuring, we discuss the OTFT performance for different channel lengths from 100 μm down to 2.7 μm. In particular, we show that lithography processing gives rise to increased contact resistances. Apart from that, mobility of C60 as material parameter is only weakly affected which underlines the compatibility of the suggested structuring procedure. The potential of this structuring procedure for future integration of driving transistors in active matrix displays is demonstrated.

1. Introduction

High density integration techniques like photo-lithography with high yields and throughput are a major reason for the commercial success of inorganic semiconductor devices. A basic requirement for such structuring procedures is either to dissolve or to etch the photo-resist by solvents or etchants which are benign to the semiconductor material. For inorganic semiconductors one benefits from insolubility of these materials to most polar and non-polar solvents as well as from their natural resistivity against etchants.

In context of organic semiconductors, there is an increasing interest in suitable techniques for high density integration of OTFTs, e.g. for drivers in active matrix displays [1] or organic microprocessors [2]. Various methods for structuring of organic semiconductors like shadow mask deposition, laser ablation, inkjet printing, or nano-imprinting have been suggested. However, they are either leaking in their throughput capacitance, accessible feature size, or their compatibility with the organic compounds itself. Photo-lithography on the other hand is a very powerful technique which is currently adopted as main stream patterning approach for inorganic electronic industry. Photo-lithography is a relatively simple, high-throughput, cost effective, extremely reproducible and controllable high resolution patterning technique with well established registration protocols. Despite all the advantages of photo-lithography, it is generally inappropriate for organic semiconductors since organic materials are sensitive to photo-resist, developer and lift-off solvents. Nevertheless, several successful approaches on structuring organic semiconductors employing photo-lithography have been reported. In some limited cases, commercial resist/solvent combination were proven to be compatible with organic semiconductors [3,4]. This approach is mostly suitable for a few robust hole transporting polymer semiconductors, which are resistant to polar organic solvents used in traditional photo-lithography (e.g., PGMEA – propylene glycol methyl ether acetate).

* Corresponding author.
E-mail address: hans.kleemann@iapp.de (H. Kleemann).
URL: http://www.iapp.de (H. Kleemann).

1566-1199/$ - see front matter © 2011 Elsevier B.V. All rights reserved.
doi:10.1016/j.orgel.2011.12.009

Another successful approach to address this issue is to use photo-crosslinkable organic semiconductors [5,6]. This is a very powerful approach since it allows easy patterning of the organic film itself and also allows patterning of the next layers, since crosslinked material becomes more robust against further wet chemical processing. However, the disadvantage of this approach is that it requires a special synthesis of the material. Tailoring materials to be photo-crosslinkable and to have good electronic properties appears to be very challenging.

Few other approaches rely on using sacrificial protection layers, which can protect active material from the wet chemical during the lithographic process and can be either removed or left as a functional part of the device [7–10].

In this contribution, we use the latter approach due to its versality and potential compatibility with a wide class of organic semiconductors. Furthermore, well establish conventional photo-lithographic protocols can be used. We chose highly fluorinated lift-off resist in combination with conventional positive imaging resist to show the ability for structuring source and drain electrodes of an *n*-channel OTFT directly on top of the buckyball C60 molecule. As we will point out, the proposed lithography protocol allows for processing under ambient conditions which greatly simplifies the process. We furthermore compare shadow-mask patterned reference OTFTs to fully lithography processed transistors in regard to mobility, contact resistance, subthreshold-swing and threshold voltage. Employing this patterning technique, we varied the channel length by nearly two orders of magnitude from 100 μm to 2.7 μm. In particular, we will point out that for our short channel devices, neither a contact resistance limitation nor typical short channel effects (e.g. vanishing of the saturation regime) are obtainable. Reports on bottom-contact OTFTs [11,12], however, unambiguously show that such short channel effects appear already at considerable larger channel lengths of several micrometers depending on the used semiconductor material. Ante et al. [13], however have recently reported that even for a channel length of 150 nm, no short channel effects are observed in top-contact OTFTs. They show that such devices are limited by contact resistance, which can partially be overcome by molecular interface doping. In contrast to Ante et al., we are not able to reach a contact limitation of our devices. For our top-contact OTFTs we show that this is related to the characteristic overlap length between gate and source/drain electrode, over which charge flow between contact and semiconductor mainly occurs. This so-called transfer length, which is also a part of the active channel region, dominates OTFT performance for short channel devices. In particular, we show that an increased contact resistance related to the lithographical structuring leads to strong deviations in scaling behavior of OTFTs. Such effects require further consideration for high-density integration of OTFTs e.g. for active matrix displays. Nevertheless, we are able demonstrate that by using this patterning technique, one can attain sufficient currents to drive a significant larger organic light emitting diode (OLED) at a luminance of more than 1000 cd/m^2 for driving voltages of 12 V.

2. Experimental

OTFTs studied in this contribution are fabricated on highly doped silicon substrates covered by a 50 nm thick layer of Al_2O_3 produced by atomic layer deposition (dielectric constant 7.8). Substrates are cleaned using acetone, ethanol, and isopropanol for 5 min in a supersonic bath. Afterwards samples are exposed to oxygen plasma for 10 min and dipped into Hexamethyldisilazane (HMDS, 30 min at room temperature) for surface passivation. Spin rinsing using isopropanol is employed to remove residuals of HMDS. C60 (40 nm, 0.03 nm/s) as active material and gold (35 nm, 0.1 nm/s) as source and drain electrode are deposited on these substrates under vacuum conditions (base pressure 10^{-7} mbar). Deposition rates are controlled by quartz crystal monitors. Our lithography procedure is based on a bilayer resist concept. The protocol is illustrated in Fig. 1. A first layer of lift-off resist (*Ortho*310 – negative resist, Orthogonal Inc.) is spin-coated (1000 rpm, 30 s) under ambient conditions directly on C60 (see Fig. 1b). The role of *Ortho*310 film is twofold. First, it acts as a protective resist since it is based on fluorinated photosensitive polymers which are chemically benign to non-fluorinated organic compounds. It is processed (deposited, etched, and stripped off) by hydrofluoroether (HFE) solvents. The advantage of HFE solvents is their general compatibility with wide class of organic semiconductors, including polymers and small molecules [14]. The second role of *Ortho*310 is its use as lift-off resist. This is possible due to mutual orthogonality of *Ortho*310 and non-fluorinated commercial imaging resist. Thus processing of *Ortho*310 does not influence the imaging resist and vice versa. An imaging resist (*ma* – *P*1210, positive resist from micro resist technology GmbH, Berlin) is spin coated onto *Ortho*310 using the same procedure. The samples are exposed by a SF-100 UV broadband exposure system (Fig. 1b). The exposed parts of *ma* – *P*1210 are removed by development in *NaOH* (Fig. 1c) and rinsing in DI-water. In this way *ma* – *P*1210 serves as an etching mask for *Ortho*310. The pattern of *ma* – *P*1210 resist is transferred to *Ortho*310 by spin-etching with *HFE*7300 solvent (Fig. 1d). Gold film is deposited as described through the resist stencil and finally spare gold is removed via lift-off using HFE 7100 in a nitrogen atmosphere (Fig. 1e and f). Apart from (f), all other steps of the structuring protocol are done under ambient conditions in air.

For reference, we produced OTFTs with top-contact electrodes by shadow mask deposition. OTFTs are characterized by a HP 4145B parameter analyzer in a nitrogen glovebox. To avoid effects of charging we utilized a measurement procedure with a gate and source–drain voltage refresh time of 3 s.

X-ray photoelectron spectroscopy (XPS) measurements are performed with a Phoibos 100 system (Specs, Berlin, Germany) in UHV with a base pressure of 10^{-10} mbar. The sample for XPS investigations is prepared on a cleaned glass substrate, which is covered by a 15 nm thick film of gold. On this gold layer we deposited a 15 nm thick layer of C60. Afterwards, photoresist is coated, exposed and removed as described by the lithography protocol for OTFT

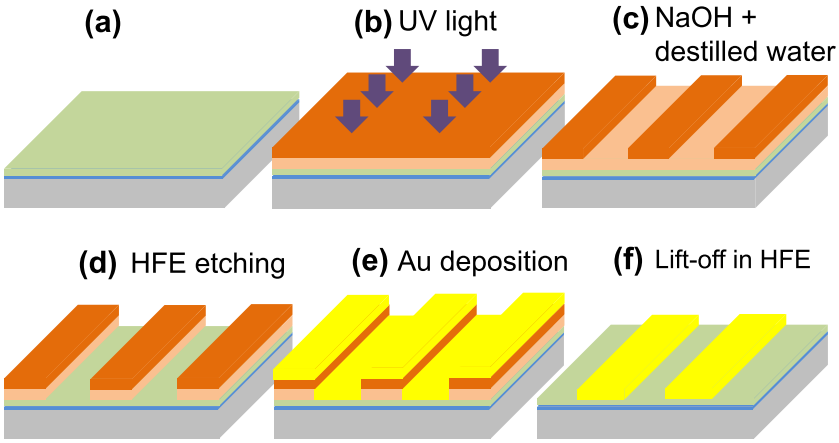

Fig. 1. Schema of the patterning procedure containing (a + b) exposure (c) development, (d) etching), and lift-off (e + f) steps. The layers are: silicon backgate (light grey), Al_2O_3 (blue), C60 (green), *Ortho*310 (light orange), ma-P1210 (orange), and gold (yellow). (For interpretation of the references to colour in this figure legend, the reader is referred to the web version of this article.)

preparation. Thus, this sample is comparable to our OTFT devices before deposition of the source/drain electrode. For X-ray excitation, we use an Al K_α X-ray source at 1486.6 eV with a resolution of 400 meV. The spectra are fitted with the free software XPSPeak41v [15].

The OLED used here to demonstrate the applicability of the structuring procedure for driving transistors is prepared as described elsewhere [16]. The active area of the OLED is 6.49 mm^2.

3. Results and discussion

For this study we chose the buckyball C60 molecule, since this material can be seen as a benchmark material for electron transporting organic semiconductors. Its high symmetry leads to highest mobility values reported for electron transporting organic semiconductors [17–21]. However, C60 has the same tendency as most other electron transporting organic semiconductors: water and oxygen can be adsorbed easily and can act as trap states for charge carrier transport [22]. To discuss influences of the lithography on OTFT performance we consider changes in threshold voltage, contact resistance, mobility and subthreshold-swing in comparison to a reference device structured by shadow mask.

In the present study, we discuss photo-lithographically produced *n*-channel OTFTs in comparison to reference devices. For C60 electron mobilities up to 5 $cm^2/(Vs)$ have been reported [18,19,21] using special surface treatments or low work-function metals for source and drain electrodes. OTFTs in this study are not optimized for highest charge carrier mobility. Nevertheless, charge mobilities obtained in this work are within the state of the art for C60 OTFTs and they can be further improved as suggested by Zhang [18,19] and Virkar [21].

The influence of lithographic structuring on OTFT can have two reasons. On the one hand, resist and solvent compounds will interact with the organic semiconductor. On the other hand, there is an influence since we expose the samples for several minutes to air and moisture before they are covered by the photo-resist. In order to distinguish between these two influences, we exposed the reference sample and the lithographically processed devices to air and performed additional annealing steps. In detail, after processing and the first measurement of fresh devices, the samples have been exposed to air for one hour without protective resist and have been heated afterwards for 1 h in a nitrogen glovebox at 100 °C.

It is well know that C60, which has been exposed to air can be reactivated in an oxygen-free atmosphere [22,23] (nitrogen glovebox or vacuum). Additional heating reduces the required reactivation time. As shown by Matsushima et al. [22] C60 contains two dominant trap levels. A deep one (0.4 eV below the conduction level) and a shallow one (0.2 eV below the conduction level), which is mainly caused by physisorption of oxygen and water. These shallow trap states can be healed by heating under vacuum conditions or inert atmosphere. Accordingly, our post-annealing step should help to remove all residuals of water and oxygen remaining in C60. Thus, changes of OTFT parameters (threshold voltage, contact resistance, mobility) that can reversed the annealing procedure are likely caused by the accidental influence of water and oxygen.

3.1. Comparison of threshold voltage and subthreshold-swing

In Fig. 2 we show transfer characteristics and current–voltage curves (inset) of a fully lithography structured OTFT in comparison to a reference device. In general, both devices show typical OTFT performance, which means a clear off-state, a linear regime and a saturation if V_{DS} exceeds $V_G - V_{th}$. Nevertheless, there are clear differences between the reference OTFT and lithographically structured OTFTs. Obviously, there is a shift in threshold voltage, and a reduced on-state current.

In detail, the threshold voltage is shifted between fresh reference sample ($V_{th} = 1.4$ V) and fully lithography produced sample ($V_{th} = 2.3$ V) by 0.9 V (values are summarized in Table 1). The threshold voltage of the lithographically produced sample further increases to $V_{th} = 3.8$ V if we exposure the sample to air for one hour

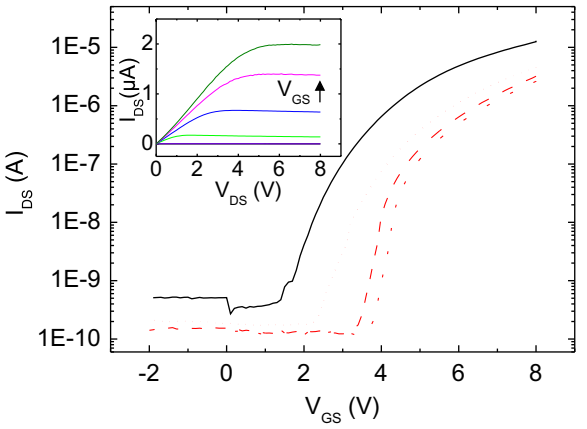

Fig. 2. Transfer characteristics ($V_{DS} = 8$ V) of lithographically (red) and shadow mask patterned (black) C60 OTFTs. The transistors have a channel length of 30 μm and a channel width of 300 μm, respectively. The red short dotted curve denotes the performances directly after deposition. The red dotted curve shows OTFT performance after one our under ambient conditions (measurement in nitrogen) and the red dashed line after an annealing of one hour at 100 °C in a nitrogen glovebox. The inset shows the current–voltage characteristics of the lithographically processed device. The gate voltages are: 2 V (violet), 3 V (light green), 4 V (blue), 6 V (magenta), 8 V (dark green). (For interpretation of the references to colour in this figure legend, the reader is referred to the web version of this article.)

and anneal it afterwards ($V_{th} = 3.4$ V). Thus, oxygen exposure increases threshold voltage. This can be partially compensated by heating. Focusing on the reference sample, however, we obtain a similar tendency of threshold voltage shift. After air exposure, we measured a threshold voltage of 3.3 V and a reduced value of 2.3 V after annealing. The threshold shift likely arises because of water adsorbed at the dielectric interface [24]. These states, acting also as trap states, are not accessible by the simple annealing procedure, which is related to the strong binding of hydroxyl groups onto the insulator material. Utilizing highly hydrophobic gate dielectrics as e.g. polymers might help to reduce this effect. Differences in total values of threshold voltage likely arise from fact, that OTFTs produced by lithography have been exposed to air for a longer time and no annealing has been employed after structuring.

Furthermore, a comparison of the transfer curves and on-state currents suggests, that the transfer curve of the lithographically produced sample is merely parallel shifted for $V_{GS} > 5$ V. Accordingly, mobility determined in this OTFT geometry is only slightly influenced (see Table 1). This indicates that the transport properties of C60 are slightly affected and annealing is sufficient to remove oxygen and water related trap states in C60. Apart from this, for $V_{GS} < 5$ V a steeper rise of the transfer curve is observed for the lithography produced samples. This increase in subthreshold-swing becomes more pronounced for larger threshold voltages (see Table 1). In contrast to that, the subthreshold-swing of the reference device (fresh; 1 h air; annealing at 100 °C for 1 h) is slightly affected (580 mV/dec; 600 mV/dec; 610 mV/dec) in comparison to lithographically made samples. However, by adopting that threshold shift is the only influence of lithographic structuring, changes in subthreshold-swing cannot be explained consistently. However, as we will point out, this can be explained by the fact that lithographic structuring leads to an increase of contact resistance.

3.2. Comparison of contact resistance and mobility

The ON state current for lithographically made samples is smaller than for the reference sample. Besides mobility, an important parameter which may affect the ON state of the field effect transistor is the contact resistance (R_c). We determine R_c using a transmission line model [25] for all tested type of devices. As shown in Fig. 3, we evaluate the contact resistance from a channel length variation between 30 μm and 100 μm. The gate-source voltage dependence (inset) of the contact resistance indicates a field dependent injection mechanism. Table 1 shows that lithographically made samples exhibit a stronger field dependence of contact resistance than the reference. We obtain for lithographically made samples a contact resistance four to five times larger than for the reference device. The contact resistance obtained for the reference device is in accordance to previously reported values [18]. Lithographically made OTFTs exhibit a contact resistance above this previous report by a factor of two.

For low source-gate voltages, we obtain for different post-treatment steps significant differences in contact resistance for lithographically procuded samples. Since we do not correct contact resistance with regard to threshold voltage, these differences likely arise because of the threshold shift for the various post-treatment steps. However, for a source-gate voltage of 8 V the contact resistance

Table 1
Threshold voltage, contact resistance, and mobility for reference C60 OTFT and the fully lithography processed transistors. The mobility and threshold voltage are determined for long channel devices (channel length 30 μm). Mobility is taken from the slope of the transfer curve at $V_{GS} = 5$ V. The standard deviations are taken from variations of 3 OTFTs for each channel length and from fitting using the transmission line method, respectively.

	V_{th} (V)	Contact resistance (kΩ cm)			Mobility (cm^2/Vs^{-1})	Subthreshold-swing (mV/dec)
		$V_{GS} = 4$ V	$V_{GS} = 6$ V	$V_{GS} = 8$ V		
Reference (fresh)	1.4 ± 0.1	8.9 ± 0.8	6.8 ± 0.8	6.1 ± 0.5	0.17 ± 0.02	580 ± 20
Reference (1 h air)	3.3 ± 0.1	22.3 ± 1.6	14.0 ± 1.2	11.4 ± 1.1	0.14 ± 0.02	600 ± 20
Reference (1 h at 100 °C)	2.3 ± 0.1	14.4 ± 1.4	10.5 ± 1.2	8.3 ± 0.7	0.15 ± 0.02	610 ± 20
Lithography (fresh)	2.3 ± 0.1	43.7 ± 12.5	34.5 ± 8.5	30.1 ± 3.4	0.13 ± 0.02	510 ± 20
Lithography (1 h air)	3.8 ± 0.1	96.5 ± 11.7	46.8 ± 5.6	30.7 ± 3.6	0.10 ± 0.02	280 ± 40
Lithography (1 h at 100°C)	3.4 ± 0.1	71.6 ± 6.1	38.2 ± 3.8	22.7 ± 4.1	0.11 ± 0.02	250 ± 40

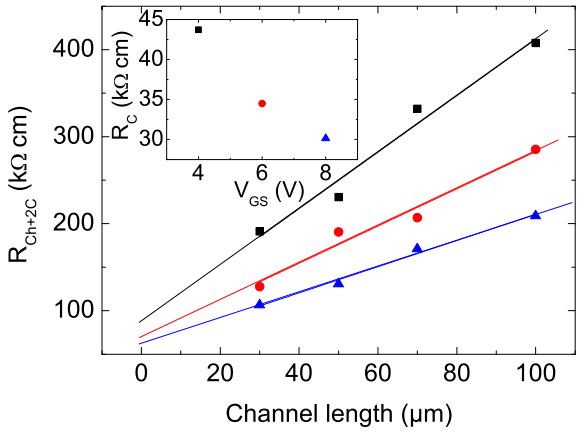

Fig. 3. Transistor resistance R_{Ch+2C} (channel + contact) of lithography produced OTFTs for different channel lengths ($V_{DS} = 2$ V). The colors denote different gate-source voltages: $V_{GS} = 4$ V (black rectangles), $V_{GS} = 6$ V (red circles), and $V_{GS} = 8$ V (blue triangles). The contact resistance R_C (inset) is estimated from the intersection at zero channel length. (For interpretation of the references to colour in this figure legend, the reader is referred to the web version of this article.)

of lithographically produced OTFTs is almost independent of the post-treatment step. Thus, for such a considerable large source-gate voltage there is almost no influence of the threshold voltage on the contact resistance. In consequence, since we obtain for all post-treatment steps similar values of contact resistance for $V_{GS} = 8$ V, we deduce that there is almost no effect of air and water related trap states in C60 on R_c. Accordingly, we conclude that the increased R_c is a direct consequence of the lithographic patterning. It likely appears because of resist residuals between the semiconductor and the source/drain electrode. This is confirmed by XPS investigations (see Fig. 4 for spectra, technical details are described in the experimental section). We obtain a XPS signal that can be attributed to fluorine, which is a main component of photo-resist and solvent used here. Consequently, there are partial solvent/resist residuals on the C60 film. For comparison we also show the Carbon related XPS signal for a pristine C60 film and a C60 film as processed for lithographically manufactured OTFTs. In detail, the signal of the C 1s core level of the pristine C60 film could be fitted with one main peak at 284.8 eV, which is generally attributed to pure carbon compounds [26], and several shake peaks generally observed for C60 [27]. In comparison, the signal of the C60 film after removing *Ortho*310 has slightly changed. We observe one additional peak at 292.1 eV. This is in range of reported CF_2 and CF_3 bonds, so this peak can be attributed to carbon, which is directly bound to fluorine. The main peak is broadened indicating that two states are present, one again at 284.8 eV and a second with a small chemical shift of 0.2 eV. We assign this shifted peak to carbon atoms in the resist, which are not directly bound with fluorine but affected by its strong electronegativity. Due to this and presence of fluorine signal we conclude that there is still some resist left after removal. However, the presence of unaffected C–C signal, attributed to the pristine C60 signal, indicates that the thickness of these residuals should be in the range of a few monolayers [28].

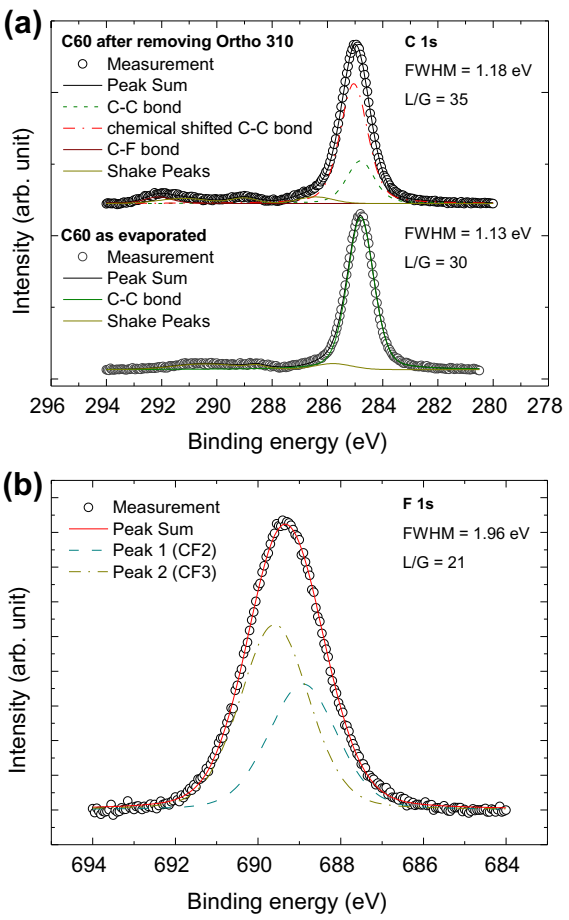

Fig. 4. (a) XPS measurements of the C 1s signal of a C60 film after removing *Ortho*310 in comparison to a C60 film as evaporated and (b) the F 1s signal of a C60 film after removing *Ortho*310. The spectra are fitted with multiple peaks, assuming a full with at half maximum (FWHM) in the range of 1.0–2.0 eV and a Lorentzian to Gaussian contribution (L/G) between 20 and 40. A Shirley background is subducted in all graphs.

However, XPS investigations clearly disclose the presence of resist residuals on the C60 film. This can particularly be seen in the determined value of mobility, which slightly differs for the reference and the lithographically made sample (see Table 1). Electron mobility of C60 obtained in this study is lower compared to previous reports [18,19,21]. This is presumably related to a surface treatment and metal electrodes not optimized [18,19,21] for highest charge carrier mobility. The photo-lithographic patterning, however, does not provide any restricting concerning usability of such special surface treatments and metal electrodes. Accordingly, they can be employed to further increase charge carrier mobility.

The effect of a reduced mobility for annealed samples is likely caused by an increased threshold, similar to contact resistance. A correction of mobility and contact resistance for threshold voltage [29] has not been made here. The problem of resist residuals is common for photo-lithography procedures. Such residuals are typically removed by descum oxygen plasma etch process. Unfortunately, in

our case such processing cannot be directly applied to organic semiconductors, due to oxidation of C60.

We conclude that lithographically made samples show an increased threshold voltage caused by air and moisture exposure during processing. This threshold likely arises because of water and oxygen related trap states at the dielectric interface. Furthermore, we deduce a sufficient healing of C60 by vacuum/glovebox annealing, which can be seen in an almost unaffected mobility (parallel shifted transfer curve for $V_{GS} > 5$ V). However, we obtain an increased contact resistance caused by resist residuals on C60. A strong field dependence of contact resistance for lithographically made samples likely causes a steeper subthreshold-swing.

3.3. Short channel devices

The ability of lithographic structuring of top contact OTFTs opens the pathway for high-density integration of such transistors. Thereby, a reduced channel length is required to achieve high on-state currents. However, contact resistance and transfer length L_0 effects [30–33,13] (length over which charge flow between contact and semiconductor mainly occurs, see inset Fig. 6) strongly restrict the maximum on-state current that one can attain. Especially the transfer length L_0 governs the active channel length for short channel devices [31,13]. For top-contact OTFTs containing a structured gate electrode, the transfer length is restricted by the geometrical overlap between source/drain and gate [13]. In case of an unstructured gate electrode, however, this transfer length can become significant and easily exceed the geometrical channel length. A main parameter influencing this transfer length is contact resistance [30].

We varied the geometric channel length L of our OTFTs from 100 μm down to 2.7 μm to study effects of increased contact resistance and transfer length. We determine the mobility for these devices since the dependency of mobility on channel length helps to disclose the transition from long channel to short channel devices. Fig. 5 displays the transfer characteristics and the source–drain voltage sweep of a 2.7 μm channel length OTFT. We obtain a linear regime for small source–drain voltages followed by a clear saturation regime. Short channel devices typically exhibit for small source–drain voltages a non-linear behavior of the source–drain current [11], which is related to the dominant contact resistance. For larger source–drain voltages a linear behavior of source–drain current instead of a saturation has been reported [11]. This is related to an increasing depletion at the drain electrode and therefore to an reduced active channel length. However, we obtain neither a strong contact limitation nor a linear regime for higher voltages.

Presumably this is caused by the fact, that the transfer length in this devices is larger than the geometric channel length. As Ante et al. [13] recently reported, the transfer length for OTFTs with structured gate is in the range of 11 μm and it is increased for larger contact resistance. Thus, we presume that transfer length is significantly larger in our case (Extrapolation of transmission line analysis [12] (see Fig. 2) suggests a transfer length in the range of 25–35 μm). Consequently, for evaluation of the mobility we expect a strong drop of its value if the channel length is equal or less than the transfer length. Fig. 6 shows the

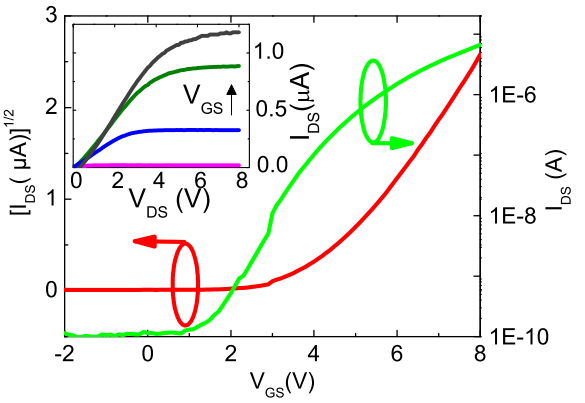

Fig. 5. Transfer characteristics ($V_{DS} = 8$ V) of a lithography produced OTFT having a geometric channel length of 2.7 μm. The inset shows the current–voltage curve for different gate voltages. Colors denote the following gate-source voltages: 2 V (magenta), 4 V (blue), 6 V (dark green), and 8 V (dark gray). (For interpretation of the references to colour in this figure legend, the reader is referred to the web version of this article.)

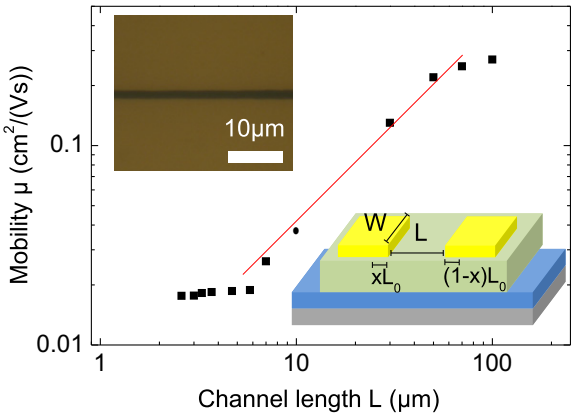

Fig. 6. Mobility for lithographically produced OTFTs for different geometric channel lengths determined in the saturation regime. The width of the source and drain contacts is 500 μm and thus it is significantly larger than the estimated transfer length. The upper inset display a photograph of the 2.7 μm channel. The lower inset shows a schema of an OTFTs, where measures as discussed in the main text are clarified.

mobility of devices with a channel length L ranging from 2.7 μm to 100 μm. We can identify three parts of that curve: (I) mobility is almost independent of channel length (long channel device, 50–100 μm), (II) a drop of mobility by a factor of 20 (transition region, 7–50 μm), and (III) a almost channel length independent mobility for very short channels (transfer length dominated, <7 μm). This behavior of the mobility is understandable if we consider the transfer length as an active part of the channel.

Usually, mobility μ as displayed in Fig. 6, is determined by the slope of the transfer curve by

$$\mu = \frac{2}{Wc} \cdot \left(\frac{\partial I_{DS}^{1/2}}{\partial V_{GS}} \right)^2 \cdot L, \qquad (1)$$

where W is the channel width and c the specific capacitance of the insulator. This assumes a geometrical channel

length L as active channel region. However, this neglects the role of transfer length L_0 as an active part of the channel. Wang et al. [33] and Benor et al. [34] studied OTFT performance within the crowding current model [31] which describes transfer length effects. They have shown that the transfer length causes an additional resistance that has the same form as the channel resistance within the saturation regime of the OTFT. Thus, in this approach the current through such an OTFT can be expressed by the formulas derived within the gradual channel approximation where merely the geometrical channel length L needs to be replaced by the effective channel L_{eff} which takes the transfer length into account.

Consequently, Eq. 1 can to be corrected by

$$\mu_{\text{long}} = \frac{2}{Wc} \cdot \left(\frac{\partial I_{\text{DS}}^{1/2}}{\partial V_{\text{GS}}} \right)^2 \cdot L_{\text{eff}}, \tag{2}$$

where μ_{long} denotes the long channel device mobility for $L \gg L_0$. Thus, we can deduce from Eqs. 1 and 2

$$\mu = \mu_{\text{long}} \left(1 - \frac{L_0^2}{(L + L_0)^2} \right), \tag{3}$$

as a channel length dependent mobility correction [34]. For sake of simplification, this derivation implies that transfer length can be treated as active part of the channel in sense of the gradual channel approximation.

However, we obtain that for a channel length $L > 50$ μm the active channel length is governed by its geometrical value and accordingly mobility μ is almost constant. For a length between 7 μm and 50 μm, the contribution of transfer length as an active part of the channel is increased. According to Eq. 3, we obtain for such devices a reciprocal channel length dependence as indicated by a red line in Fig. 6. For a channel shorter than 7 μm, the channel length is predominantly given by the transfer length L_0 resulting in a reduced mobility of 1/20 of its original value as determined for long channel devices. Relying on the gradual channel approximation, it is expected that the mobility should continuously decrease for a reduced geometrical channel length. Since this is in contradiction to our results (mobility is almost constant for $L < 7$ μm), we conclude that the transfer length cannot be treated as an active part of the channel as considered by the gradual channel approximation.

Nevertheless, Eq. 3 can qualitatively describe the obtained behavior of mobility for short channel devices structured by the lithography technique proposed here. From the transition between long channel mobility ($L > 50$ μm) and reciprocal channel length dependent mobility (7 μm $< L <$ 50 μm) we can graphically give an estimation for the transfer length of $L_0 = 30$–40 μm. However, for a more precise quantitative analysis a more sophisticated model of transfer length as well as more experimental data points are required.

3.4. Driving OTFTs for OLED-display applications

To demonstrate the capability of lithographically produced OTFTs, we show a green OLED driven by such an OTFT. We employ a transistor with a channel length of 30 μm and a channel width of 24 mm. The ratio between active area of the OLED and the driving transistor is larger than 4 in this case (including OTFT contact pads). This ratio can be increased for smaller feature sizes since the photolithography techniques enables to scale down the OTFT size.

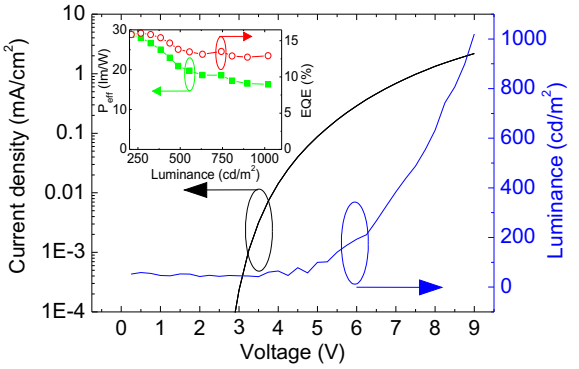

Fig. 7. OLED driven by an OTFT. The black curve shows the current through of the OLED for different gate voltages. The blue curve displays the luminance of the OLED driven by the OTFT. The inset shows external quantum efficiency (EQE, red curve, open circles) and power efficiency (P_{eff}, green curve, closed rectangles) for different luminance values. (For interpretation of the references to colour in this figure legend, the reader is referred to the web version of this article.)

We measured the luminance of the green OLED for different gate-source voltages at a fixed source–drain voltage of 12 V. The higher source–drain voltage in contrast to Fig. 1 is required to obtain the saturation regime of the OTFT with the OLED in series. Nevertheless, the highly efficient OLED used here guarantees a minimum of driving voltage, where a luminance of 1000 cd/m^2 is achieved for voltages less than 4 V (voltage drop across the OLED). As shown in Fig. 7, we obtain an increase in luminance for increasing gate voltage and 1000 cd/m^2 are exceeded at 9 V. This clearly shows that even without aggressive scaling of driving OTFTs, sufficient luminance of OLED pixels can be achieved.

4. Conclusion

Organic thin film transistors comprising C60 are fabricated by a direct photo-lithography lift-off process on the organic material under ambient conditions. We have shown that the patterning technique used here is competitive to shadow mask production in terms of OTFT performance. Structuring under ambient conditions leads to an increased threshold voltage which is presumably related to adsorption of water and oxygen at the dielectric interface. The lithographic procedure itself causes an increased contact resistance originated by residuals of resist/solvent. Heating in nitrogen atmosphere is a suitable way to reduce threshold voltage and contact resistance. The capability of the lithographic structuring technique is shown for OTFTs with channel length down to 2.7 μm. We disclose, that even for such small channels the contact resistance is not the limiting factor for OTFT performance. It is restricted

by the transfer length, which is caused by the overlap between gate and source/drain contact. However, we presume a direct relation between contact resistance and transfer length and accordingly we intend to study in further experiments the impact of contact resistance on transfer length to see, whether further reduction of contact resistance by post-annealing steps leads to an improved behavior of short channel devices.

In conclusion, we have also demonstrated that photolithographic structuring of small molecule organic semiconductor is a suitable technique for future high density and high performance integration of organic thin film transistor as e.g. driving transistors in active matrix OLED displays.

Acknowledgments

The authors thank Novaled AG and the state of Saxony for financial support in project NKOE (12712) and the BMBF through the InnoProfile Project (03IP602). A.A. Zakhidov acknowledges support of Alexander von Humboldt Foundation.

References

[1] L. Zhou, S. Park, B. Bai, J. Sun, S.-C. Wu, T. Jackson, S. Nelson, D. Freeman, Y. Hong, J. IEEE Electron. Dev. Lett. 26 (2005) 640.
[2] K. Myny, E. van Veenendaal, G. Gelinck, J. Genoe, W. Dehaene, P. Heremans, in: Solid-State Circuits Conference Digest of Technical Papers (ISSCC), 2011, IEEE International 2011, pp. 322–324.
[3] C. Balocco, L. Majewski, A. Song, Org. Electron 7 (2006) 500.
[4] J. Huang, R. Xia, Y. Kim, X. Wang, J. Dane, O. Hofmann, A. Mosley, A. de Mello, J. de Mello, D. Bradley, J. Mater. Chem. 17 (2007) 1043.
[5] C. Müller, A. Falcou, N. Reckefuss, M. Rojahn, V. Wiederhirn, P. Rudati, H. Frohne, O. Nuyken, H. Becker, K. Meerholz, Nature 421 (2003) 829.
[6] A. Afzali, C. Dimitrakopoulos, T. Graham, Adv. Mater. 15 (2003) 2066.
[7] I. Kymissis, C. Dimitrakopoulos, S. Purushothaman, J. Vac. Sci. Technol. B 20 (2002) 956.
[8] J. DeFranco, B. Schmidt, M. Lipson, G. Malliaras, Org. Electron 7 (2006) 22.
[9] J.-F. Chang, H. Sirringhaus, Adv. Mater. 21 (2009) 2530.
[10] B. Dhar, G. Kini, G. Xia, B. Jung, N. Markovic, H. Katz, J. PNAS 107 (2010) 3972.
[11] J.N. Haddock, X. Zhang, S. Zheng, Q. Zhang, S.R. Marder, B. Kippelen, Org. Electron 7 (2006) 45–54.
[12] Y. Chen, I. Shih, J. Mater. Sci. 44 (2009) 280–284.
[13] F. Ante, D. Kälblein, U. Zschieschang, T. Canzler, A. Werner, K. Takimiya, M. Ikeda, T. Sekitani, T. Someya, H. Klauk, Small 7 (2011) 1186–1191.
[14] A. Zakhidov, J.-K. Lee, J. DeFranco, P. Taylor, M. Chatzichristidi, C. Ober, G. Malliaras, Adv. Mater. 20 (2008) 3481.
[15] <www.wsu.edu/scudiero>.
[16] G. He, D. Gebeyehu, A. Werner, M. Pfeiffer, K. Leo, Proc. SPIE 26 (2004) 5464.
[17] S. Kobayashi, T. Takenobu, S. Mori, A. Fujiwara, Y. Iwasa, Sci. Technol. Adv. Mater. 4 (2003) 371.
[18] X.-H. Zhang, B. Kippelen, J. Appl. Phys. 104 (2008) 104504.
[19] X.-H. Zhang, B. Kippelen, Appl. Phys. Lett. 93 (2008) 133305.
[20] M. Kitamura, Y. Arakawa, Appl. Phys. Lett. 95 (2009) 023503.
[21] A. Virkar, S. Mannsfeld, J. Oh, M. Toney, Y. Tan, G. Liu, J. Scott, R. Miller, Z. Bao, Adv. Mater. 19 (2009) 1962–1970.
[22] T. Matsushima, M. Yahiro, C. Adachi, Appl. Phys. Lett. 91 (2007) 103505.
[23] S. Fujimori, K. Hoshimono, S. Fujita, S. Fujita, Solid State Commun. 89 (1994) 437.
[24] D. Kumaki, T. Umeda, S. Tokito, Appl. Phys. Lett. 92 (2008) 093309.
[25] P. Necliudov, M. Shur, D. Gundlach, T. Jackson, Solid State Electron 47 (2003) 259–262.
[26] B. Crist, Crist BV. Handbooks of Monochromatic XPS Spectra: The Elements and Native Oxides (XPS International LLC, 2004).
[27] C. Enkvist, S. Lunell, B. Sjogren, S. Svensson, P.A. Bruhwiler, A. Nilsson, A. Maxwell, N. Martensson, Phys. Rev. B 48 (1993) 629.
[28] D. Briggs, M. Seah, Practical Surface Analysis, John Wiley and Sons, Chichester, 1983.
[29] R. Schroeder, L. Majewski, M. Grell, Appl. Phys. Lett. 83 (2003) 3201.
[30] D. Gundlach, L. Zhou, J. Nichols, T. Jackson, P. Necliudovc, M. Shur, J. Appl. Phys. 100 (2006) 024509.
[31] T. Richards, H. Sirringhaus, J. Appl. Phys. 102 (2007).
[32] A. Hoppe, D. Knipp, B. Gburek, A. Benor, M. Marinkovic, V. Wagner, Org. Electron 11 (2010) 626–631.
[33] S. Wang, Y. Yan, K. Tsukagoshi, Appl. Phys. Lett. 97 (2010) 063307.
[34] A. Benor, D. Knipp, Org. Electron. 9 (2008) 209.